

## Realization of a time-scale with an optical clock

C. Grebing,\* A. Al-Masoudi, S. Dörscher, S. Häfner, V. Gerginov,

S. Weyers, B. Lipphardt, F. Riehle, U. Sterr, and C. Lisdat

*Physikalisch-Technische Bundesanstalt, Bundesallee 100, D-38116 Braunschweig, Germany*

(Dated: September 13, 2022)

Optical clocks are not only powerful tools for prime fundamental research, but are also deemed for the re-definition of the SI base unit second as they surpass the performance of caesium atomic clocks in both accuracy and stability by more than an order of magnitude. However, an important obstacle in this transition has so far been the limited reliability of the optical clocks that made a continuous realization of a time-scale impractical. In this paper, we demonstrate how this dilemma can be resolved and that a time-scale based on an optical clock can be established that is superior to one based on even the best caesium fountain clocks. The paper also gives further proof of the international consistency of strontium lattice clocks on the  $10^{-16}$  accuracy level, which is another prerequisite for a change in the definition of the second.

The international system of units (SI) is the universal base for all measurements and thus constitutes the backbone of natural sciences and engineering. The definitions themselves and their realizations have been adapted over the years to profit from state-of-the-art research results. Important modifications are at hand for the electrical units and the mass, which will be defined through agreed-upon values of fundamental constants [1].

Due to their impressive progress [2–8], optical clocks surpass caesium fountain clocks, which currently realize the SI-second with lowest uncertainty, in terms of stability and accuracy of the frequency realizations of the unperturbed atomic transition. This has caused discussion about the need for a re-definition of this unit [9, 10]. A first step has been the acknowledgement of suitable optical transitions in neutral atoms and ions as secondary representations of the SI unit “second” by the Comité International des Poids et Mesures (CIPM) [11].

Given the outstanding role of the SI, it is of paramount importance that adaptations must be prepared carefully. Hence, changes will be acceptable only if [9]

- an obvious candidate is identified,
- the transition is smooth, and
- the new approach is practical.

While the first point stimulates ongoing research, the second point has already been addressed satisfactorily for strontium optical lattice clocks [3, 12] by measurements of the strontium clock transition frequency with today’s best possible accuracy; the results in this paper confirm the previous measurement results. The latter prerequisite, however, has not been achieved so far for the candidate systems as existing optical clocks have generally been considered less reliable and thus less suitable for the actual implementation of a practical time-scale, which continuously accumulates the atomic seconds.

Time-scales provide us with coordinates for the position of events in time, much like a coordinate system does for the positioning in space. In particular, it needs to be realized without interruption to provide a continuous coordinate or to measure time intervals and to synchronize distant events.

Today, the Universal Coordinated Time-scale UTC is post-processed from a weighted monthly average of the time kept by some 400 microwave atomic clocks around the world that are intercompared via satellite links. To obtain time whenever needed, the time labs generate local time-scales in real-time typically by steering the output frequency of a continuously running flywheel oscillator (Fig. 1), e.g. a hydrogen maser, on a monthly period

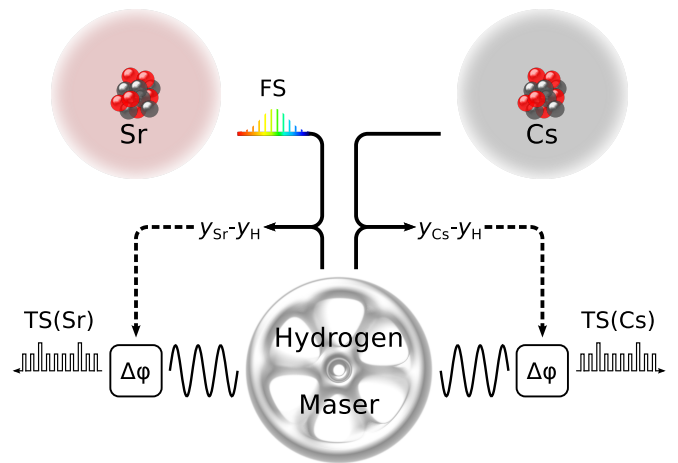


FIG. 1. Realization of a time-scale TS from a microwave and an optical clock: The Cs clock transition frequency is compared against the maser flywheel frequency. The acquired offset  $y_{\text{Cs}} - y_{\text{H}}$  is used to correct the classical time-scale TS(Cs) generated from the maser utilizing a phase stepper ( $\Delta\phi$ ). An equivalent scheme is applicable when referencing the time-scale TS(Sr) to an optical frequency standard. For that purpose, the clock laser light is down-converted to the microwave regime using a femtosecond frequency comb (FS) before comparing against the flywheel. Moreover, both maser offsets can be analysed to yield the Sr clock frequency in SI units.

\* christian.grebing@ptb.de

to stay synchronized with the UTC clock ensemble [13]. Some time labs synchronize their flywheel oscillators on an even shorter period to match the frequency of a local primary Cs clock [14].

The origin of the time error of such real-time time-scales with respect to an ideal time-scale is twofold: First, the accuracy of the local scale unit is limited by imperfections of the atomic reference(s). Even for the best caesium fountain clocks this error can integrate to about 1 ns after one month. Second, missing information from UTC or down-times of the local atomic reference clock introduce a time error depending on the instability of the flywheel oscillator.

Due to the averaging, UTC is more stable than most local time-scales. Thus, in practice the quality of a local time-scale is typically assessed by comparing to UTC, which, however, is not an ideal reference. Due to its construction, a deviation between the rate of UTC and the second of the local fountains can be as large as 0.1 ns/day, which accumulates to a time error of about 3 ns at the end of the month.

Optical clocks are expected to be capable of reducing the time error of a likewise realized local time-scale by more than one order of magnitude (time error  $\lesssim 25$  ps after a month) – provided the time error arising from their down-times is limited to an acceptable level – and thus significantly improve the time-scale’s predictability. Together with improved time link technologies [15], a network of optical atomic clocks will allow the generation of a much more stable UTC and thus labelling events in time all over the world more precisely. This would be beneficial for global navigation systems, astro- and fundamental physics.

In this article, we demonstrate how PTB’s strontium lattice clock is now able to maintain a local time-scale with a time error of less than 200 ps compared to an ideal reference over about 12 days, or  $1.6 \times 10^{-16}$  in fractional units. Over this period, the optical clock is allowed to operate with long interruptions (overall clock availability:  $\approx 30\%$ ), and down-times are bridged by a hydrogen maser flywheel. The distortion of the scale unit due to the use of the flywheel while the clock is offline causes the dominant contribution to the achieved residual time error. Yet, this shows for the first time that already today optical frequency standards with limited availability can actually serve as atomic references to support a local time-scale over extended periods, yielding a long-term performance better than of the ones referenced to the best current microwave clocks even if they are operated free of interruptions. Further improvements of the time-scale based on an optical clock are at hand by ever higher availability of the optical clock.

Moreover, the maser-flywheel-assisted Sr data together with data from one of our Cs fountains acquired in parallel enabled us to measure the Sr clock transition frequency with minimum uncertainty. So far this could only be achieved by operating the clocks for long times and/or by averaging over several of the best fountain

effect	correction	uncertainty
	$(10^{-17})$	$(10^{-17})$
BBR room	489.6	2.7
BBR oven	0.8	0.8
second-order Zeeman	3.4	0.14
cold collisions	0	0.03
background gas collisions	0.15	0.15
line pulling	0	0.01
lattice scalar/tensor	0	0.7
lattice E2/M1	0	0.5
hyperpolarisability	-0.5	0.3
tunnelling	0	0.1
probe light	0	0.01
optical path length error	0	0.01
servo error	0	0.04
DC Stark shift	0	0.2
<b>total</b>	<b>493.5</b>	<b>3.0</b>

TABLE I. Corrections applied to the measured Sr lattice clock frequency and their uncertainties during the frequency measurement given in fractional units. For a detailed description of the individual contributions the reader is referred to [12] and Sec. III.

clocks [3, 12].

## I. RESULTS

**Optical clock operation** The strontium lattice clock was operated under conditions very similar to those of a previous campaign [12]. A new interrogation laser system [16] improved the estimated optimum fractional frequency instability of the Sr clock, expressed as the Allan deviation  $\sigma$ , to below  $\sigma_{\text{Sr}}(\tau) = 2 \times 10^{-16}/\sqrt{\tau}$  with averaging time  $\tau$  [17].

For best accuracy of the lattice clock, we reduced the duty cycle of the clock interrogation and thus reduced the power dissipation in the experimental apparatus that leads to thermal gradients. These gradients limit our knowledge of the ac- and dc-Stark line shift due to black-body radiation (BBR) and thereby cause the largest uncertainty contribution to our lattice clock. With this reduced duty cycle, our clock still achieved an estimated instability of about  $\sigma_{\text{Sr}}(\tau) = 5 \times 10^{-16}/\sqrt{\tau}$  during the measurement campaign. The clock uncertainty has been evaluated similarly to [12]. The uncertainty budget is summarized in Tab. I. The systematic uncertainty  $u_B(\text{Sr})$  is thus an order of magnitude smaller than PTB’s Cs fountain clock’s uncertainty of  $u_B(\text{Cs}) = 3.1 \times 10^{-16}$  [18, 19]. Further details are given in Sec. III.

From October 6 through 15, 2014, the lattice clock was operated together with our primary Cs clock to measure the SI frequency of the Sr clock transition, which we will discuss first. The frequencies of the Cs clock and the Sr lattice clock have been compared via femtosecond-frequency combs (FS in Fig. 1). A continuously operated, high-performance hydrogen maser (VREMYA-CH VCH-1003M) used as a flywheel is connected to both clocks,

e.g. for the generation of a time-scale steered by either the Cs fountain clock (TS(Cs), [14]) or the lattice clock (TS(Sr)). During the measurement campaign, the lattice clock was operated over a total up-time of  $T_{\text{Sr}} = 267\,000\text{ s}$  (shown in Fig. 2 (b)), together with the almost continuously running fountain clock (availability > 98 %).

From this simultaneous comparison of the Cs and the Sr clock with the maser, the lattice clock's frequency can be calculated in the SI unit Hertz as realized by the Cs fountain clock. For white frequency noise, which is the dominating noise type in atomic frequency standards, the statistical clock uncertainty for a given averaging time  $\tau$  is equal to the Allan deviation  $u_{\text{clock}}(\tau) = \sigma_{\text{clock}}(\tau)$  [20]. Thus, the fountain clock's instability  $\sigma_{\text{Cs}}(\tau) = 1.7 \times 10^{-13}/\sqrt{\tau}$  clearly dominates the statistical uncertainty of the measurement given by  $u_A = \sqrt{\sigma_{\text{Sr}}^2(T_{\text{Sr}}) + \sigma_{\text{Cs}}^2(T_{\text{Sr}})} = 3.3 \times 10^{-16}$ .

However, using only the joint up-times of both clocks does not make any use of the information available from the maser: Its frequency is more stable than the fountain's for periods of up to  $10^5\text{ s}$  and can be measured accurately even during short up-times of the lattice clock. Therefore, it is reasonable to take the maser frequency value measured with the Sr clock as representative for longer intervals to improve  $u_A$ .

In general, due to the maser instability there is a potential difference between the maser frequency averaged over time  $T_{\text{Sr}}$  and an extended time  $T_{\text{ext}}$ . The lack of knowledge about this potential difference is expressed as an additional uncertainty  $u_{\text{ext}}$ , which, given the knowledge of the maser flywheel's properties, can be calculated.

**Data analysis** The uncertainty  $u_{\text{ext}}$  arises from the extrapolation of the mean flywheel frequency measured with our Sr clock over time  $T_{\text{Sr}}$  to the longer time  $T_{\text{ext}}$ . With the help of Parseval's theorem,  $u_{\text{ext}}$  can be expressed by the flywheel's spectrum of frequency fluctuations  $S(f)$  and a weighting function  $g(t)$  that describes the respective measurement intervals (see Sec. III).

The maser spectrum  $S(f)$  is extracted from different comparisons: the fast fluctuations and, thus, the stability at short averaging times  $\tau$  are obtained from a direct comparison with the Sr clock. The Allan deviation of a long continuous data set is presented in Fig. 2 (a) (triangles). Mid- and low-frequency information about the maser's frequency fluctuations are obtained from preceding maser – maser comparisons (diamonds) and the measurements against the fountain clocks (dots, circles), respectively. From these data, we derive a model for  $S(f)$  that includes flicker frequency, white frequency, and white phase noise contributions. A linear maser drift was omitted here, because the analysis was designed to be drift-insensitive (Sec. III).

The given Sr up-times  $T_{\text{Sr}}$  (see Fig. 2 (b)) and the length and distribution of the extended time  $T_{\text{ext}}$ , which we are free to choose, determine the weighting function  $g(t)$  (see Fig. 2 (c) for the exemplary case of  $T_{\text{ext}} \approx 10^6\text{ s}$ ) and, thus, together with  $S(f)$  the corresponding extrapolation uncertainty  $u_{\text{ext}}$  (inset of Fig. 2 (a)). Due to the

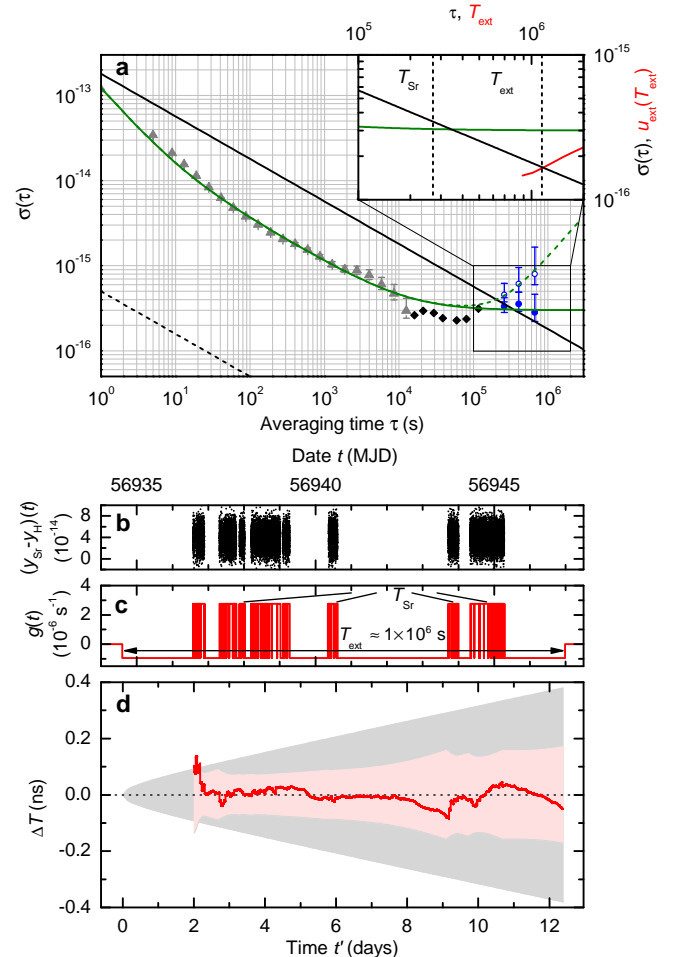


FIG. 2. **a:** Stability as represented by the Allan deviation  $\sigma$  of the relevant oscillators. Solid black line – fountain clock CSF2, dashed black line – Sr lattice clock, data points – measured maser stability (triangles: vs. lattice clock, diamonds: maser comparisons, empty dots: against fountain clocks, filled dots: ditto without linear drift), solid (dashed) green line – noise model for the maser with (without) linear drift removed. The inset again shows the stabilities of the maser (green) and fountain clock (black). The red curve shows the additional uncertainty  $u_{\text{ext}}$  when the maser is used as a flywheel and data is extrapolated from an interval  $T_{\text{Sr}} = 267\,000\text{ s}$  to  $T_{\text{ext}}$ . Dashed vertical lines indicate the direct and the optimum extrapolation measurement times. **b:** Frequency deviation between the nominal 100 MHz maser output and the Sr lattice clock averaged over 10 s assuming the Sr clock transition frequency equal to the recommendation of the CIPM for the secondary representation of the second [21], in total 267 000 s. **c:** Weighting function used to derive the calibration uncertainty of the hydrogen maser's frequency with respect to the Sr lattice clock for an interval of  $10^6\text{ s}$ . **d:** Time error of a simulated time-scale TS(Sr) (red solid line) with respect to an ideal reference. It is shown starting with the first corrected interval. The shaded areas show the  $1-\sigma$  time uncertainty range of TS(Sr) (red) and TS(Cs) (gray) including statistical and systematic contributions.

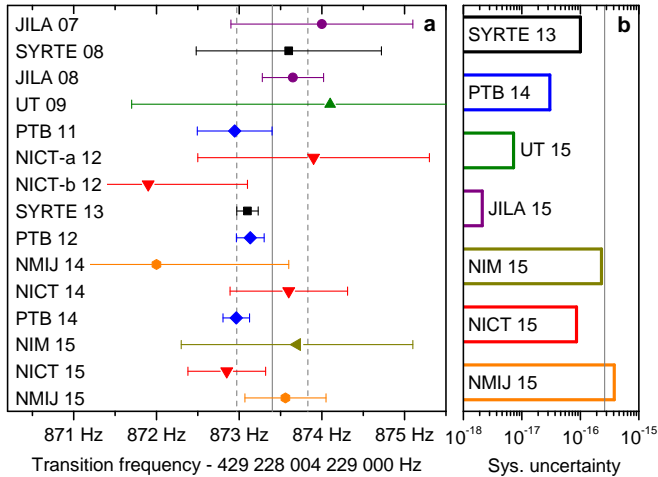


FIG. 3. **a:** Comparison of measured absolute frequencies of the  $5s^2 \ ^1S_0 - 5s5p \ ^3P_0$  transition in  $^{87}\text{Sr}$ . The values have been obtained from various references [3, 12, 22–33]. PTB 14 has been obtained in this work. The vertical line indicates the frequency recommended by the CIPM in 2013 for the secondary representation of the second by Sr lattice clocks [21], the dashed lines show the assigned uncertainty. **b:** Listing of the systematic uncertainty  $u_B$  of the best Sr clocks worldwide [3, 8, 31–34]. The gray line indicates the Cs systematic uncertainty of the absolute frequency measurement with the smallest overall uncertainty so far [3].

highly reliable Cs fountain it was not necessary to consider the influence of its down-times on  $g(t)$ .

For a flywheel-assisted Sr absolute frequency measurement we optimize  $T_{\text{ext}}$  such that the overall statistical measurement uncertainty  $u_A = \sqrt{\sigma_{\text{Sr}}^2(T_{\text{Sr}}) + \sigma_{\text{Cs}}^2(T_{\text{ext}}) + u_{\text{ext}}^2(T_{\text{ext}})}$  is minimized. As shown in the inset of Fig. 2 (a), the extrapolation uncertainty reaches the statistical uncertainty of the primary clock CSF2 at about  $10^6$  s; further extension would degrade the combined statistical uncertainty  $u_A$ . We can therefore enlarge the data set from 267 000 s to about  $10^6$  s. In consequence, the fractional systematic uncertainty of the primary fountain clock of  $u_B(\text{Cs}) = 3.1 \times 10^{-16}$  becomes the largest contribution to the overall uncertainty of this frequency measurement of our strontium lattice clock. The result for the Sr clock transition frequency is 429 228 004 229 872.97(16) Hz, which is in very good agreement with previous high-accuracy measurements [3, 12] and provides a metrologically important confirmation that is necessary to build confidence in view of a re-definition of the SI-unit second. The excellent agreement between absolute frequency measurements of strontium lattice clocks in numerous institutes is shown in Fig. 3 (a). Fig. 3 (b) points out that the systematic uncertainties of present-day Sr clocks worldwide range from similar to to well below the Cs systematics of the absolute frequency measurement with the lowest overall uncertainty ever achieved [3].

**Realizing an optical time-scale** The approach discussed here can be used not only to reduce the statistical uncertainty of frequency measurements, but also to establish a continuous time-scale from a frequency standard with an availability of considerably less than 100 %. This situation is not particular to optical clocks [32, 33, 35], but nowadays prevalent when time-scales are established in metrology institutes or contributing to UTC [13, 36, 37]. In the following, we consider the combination of the Sr lattice clock and the continuously running maser flywheel to constitute a time-scale based on an optical clock. The main difference to the absolute frequency measurement is that now we are not free to chose the extended time interval  $T_{\text{ext}}$  since it is determined by the time-scale’s origin and the duration for which the time-scale has to be provided. For convenience, we will discuss an optical time-scale that covers the 12 days of our flywheel-assisted absolute frequency measurement campaign.

The predictability of a time-scale is quantified by its uncertainty: The inset in Fig. 2 (a) shows the frequency uncertainty  $u_{\text{ext}}(T_{\text{ext}})$  of an ensemble of masers – all having the same instability like our maser – whose frequencies are extrapolated from  $T_{\text{Sr}}$  to a period  $T_{\text{ext}}$  (red line). The curve can be related to an accumulated time-scale uncertainty via  $u_{\text{ext}}^{\text{TS}} = u_{\text{ext}}(T_{\text{ext}}) \cdot T_{\text{ext}}$  when realizing a time-scale by correcting such maser’s frequency by interrupted measurements with our optical clock. To yield the overall optical time-scale uncertainty, this contribution has to be added in quadrature to the accumulated time uncertainty of the Sr clock’s scale unit, which is at least an order of magnitude smaller.

We choose a numerical approach in order to demonstrate the potential performance of a real-time steered time-scale  $\text{TS}(\text{Sr})$  during the measurement interval of interest since an experimental characterization would suffer from the instability of available reference time-scales.  $\text{TS}(\text{Sr})$  is compared to the uncertainty of a theoretical time-scale  $\text{TS}(\text{Cs})$  based on a Cs reference with 100 % up-time (assuming the parameters of PTB’s fountain clock CSF2). In order to provide time whenever needed we choose a real-time implementation even though it bears tougher constraints, which can result in a degraded instability compared to a post-processing approach.

In general, the steering algorithm can be optimized with respect to a stable scale unit and a good long-term performance. Both design goals coincide for 100 % clock up-time but they diverge the longer the clock down-times are that must be bridged with a less stable flywheel. For  $\text{TS}(\text{Sr})$  we focus on a low statistical uncertainty for long averaging times to reach the clock’s systematics as quickly as possible.

To estimate the error of  $\text{TS}(\text{Sr})$ , we numerically generate frequency data traces on a 10 s grid for the maser flywheel and the Sr clock using the time intervals of Fig. 2 (c). While the clock trace accounts for the statistical noise  $\sigma_{\text{Sr}}$ , the maser trace reflects the noise and drift characteristics of our maser model (see Sec. III).

This data is used to simulate a time-scale  $\text{TS}(\text{Sr})$  (see Fig. 2 (d), starting with the first corrected period). At the beginning of the measurement interval ( $t' = 0$  corresponds to the Modified Julian Date (MJD)  $t \approx 56934.6$ ), the time error  $\Delta T$  between the time-scale and an ideal one is set to zero. The steering algorithm works as follows: The average maser frequency is calculated regularly using the frequency information available up to that point from the Sr clock. This regular period is chosen to one hour. The average  $\bar{y}_{\text{H}} - y_{\text{Sr}}$  is used as estimate for the maser frequency  $\bar{y}_{\text{H}}$  over the full elapsed time  $t'$ . The corresponding time error is applied to the phase stepper in Fig. 1 to correct the time-scale from the maser as  $\Delta T' = -t' \cdot \bar{y}_{\text{H}}$ . To attain a complete picture, one also has to account for the Sr clock's systematics  $u_{\text{B}}(\text{Sr})$ . This is achieved by setting off the fractional clock frequency from its ideal value by  $0.5 \times u_{\text{B}}(\text{Sr})$ , which results in a minor time error of about 15 ps over the 12 days.

We observe a very stable behaviour of  $\text{TS}(\text{Sr})$  (Fig. 2 (d)); it is rather smooth and no excursions larger than 150 ps are observed. The initial transient response at day 2 is an artefact of the initialization of the real-time time-scale and could be reduced considerably in post-processing. Between day 6 and 9, when no data from the lattice clock is available,  $\text{TS}(\text{Sr})$  starts to deviate according to the free-running maser instability, but once there is new optical data available ( $t > 9$  days) the time offset does not increase further and is even reduced due to a improved estimate of the past maser average frequency.

In addition, Fig. 2 (d) shows uncertainty bands of independent time-scale realizations of  $\text{TS}(\text{Sr})$  and  $\text{TS}(\text{Cs})$  as shaded areas including statistical and systematic contributions. In case of  $\text{TS}(\text{Sr})$ , the statistical uncertainty connected to the interrupted optical clock operation  $u_{\text{ext}}^{\text{TS}}$  is calculated by the method described above, applying a weighting function that reflects the elapsed time and up-time of the optical clock. In this case,  $u_{\text{ext}}^{\text{TS}}$  is not insensitive to a linear drift of the flywheel for all times and thus an uncertainty contribution considering this fact is added in quadrature. However, in a real operation scenario the drift is usually known, e.g. from long-term comparisons against UTC, and can easily be corrected.

For the considered 12-days period, the uncertainty of  $\text{TS}(\text{Sr})$  is below 200 ps at all times. While the overall uncertainty of  $\text{TS}(\text{Cs})$  is dominated by the reference clock's systematics, that of  $\text{TS}(\text{Sr})$  is dominated by  $u_{\text{ext}}^{\text{TS}}$ . Thus, with increasing optical clock availability the uncertainty of  $\text{TS}(\text{Sr})$  would be further reduced. Yet, even with the optical clock operation periods at hand, which can be considerably increased for the realization of a time-scale, the uncertainty of  $\text{TS}(\text{Sr})$  is clearly below that of the traditional time-scale at all relevant times. Moreover, the uncertainty of  $\text{TS}(\text{Cs})$  is increasing much faster.

The formalism presented here is applicable to arbitrary flywheel-assisted clock measurement scenarios. Therefore, it allows assessing the scaling of the time errors for longer measurements. For example, when hypothetically providing  $\text{TS}(\text{Sr})$  for a longer interval by repeating

the measurement campaign illustrated in Fig. 2 (c) in a similar way, both campaigns can be considered statistically independent and, thus, the overall time error essentially increases with the square-root of the combined campaigns' total duration  $T'_{\text{ext}}$  and correspondingly the statistical extrapolation uncertainty of the average frequency scales with  $T'^{-1/2}_{\text{ext}}$ .

## II. DISCUSSION

This paper demonstrates that optical frequency standards and in particular strontium lattice clocks have reached a maturity that they now can be used in combination with a high-quality commercially available flywheel oscillator to generate a time-scale that shows beyond state-of-the-art performance. This is essential for actual optical clock applications and a redefinition of the SI-unit second. The measurement presented in Fig. 2 (b) did not explicitly aim for maximum up-time and can therefore be regarded a lower limit of capability of our apparatus. Yet, Fig. 2 (d) shows that a time error of below 200 ps was achieved for a measurement interval of 12 days. Continuation of the campaign would have led to a time error of about 300 ps over 30 days, the typical comparison duration to establish UTC. This is a remarkably low value in view of the deviations in the ns-range between the best time-scales reported in the monthly Circular-T [38], which, however, includes an additional time link error of about  $\lesssim 1$  ns.

Concerning the flywheel oscillator, several choices are available besides the H-maser used here to achieve lower scale unit distortions for certain gap durations. Cryogenic sapphire microwave oscillators [39], cryogenic optical reference resonators [40–42], and lasers stabilized by the method of spectral hole burning [43] show excellent mid- and long-term stability and could serve this purpose. Even an optical clock that is optimized for reliability instead of accuracy can be envisaged. Ultimately, an ensemble of flywheels is conceivable providing lowest instability for all occurring gap durations.

Today's satellite-based comparison techniques can readily provide time-scale comparisons with uncertainties below 1 ns [44]. Thus, having averaged for a year or more, the well-established satellite network would allow the intercontinental comparison of flywheel-assisted optical clocks in the low  $10^{-17}$  regime. Even further, ESA's future space mission Atomic Clock Ensemble in Space (ACES) will provide enhanced frequency comparison capabilities over intercontinental distances [45], such that flywheel-supported optical clock comparisons will no longer be limited by the satellite link between them. Thus, intercontinental clock comparisons with uncertainty in the  $10^{-18}$  regime after averaging over a month is within reach.

The current optical clocks can be developed towards mostly autonomous systems that will increase the average availabilities [46]. For example, a clock availability

of 70 % would immediately improve the time-scale uncertainty further to below 50 ps over 30 days assuming our system and a worst-case-scenario of a single 7 h interruption per day, which corresponds to a frequency uncertainty of  $2 \times 10^{-17}$ .

### III. METHODS

**Sr lattice clock operation** To interrogate the 698 nm  $^1S_0 - ^3P_0$  clock transition of  $^{87}\text{Sr}$ , an atomic beam from an oven is Zeeman-slowed and loaded into a magneto-optical trap (MOT) operated on the strong 461 nm  $^1S_0 - ^1P_1$  transition. After less than 300 ms loading, the atoms are transferred into a second-stage MOT operated on the 689 nm intercombination line,  $^1S_0 - ^3P_1$ , that allows for laser cooling of the atoms to a few micro-Kelvin.

During the last cooling phase, the atoms are loaded into a nearly horizontally oriented 1D-optical lattice at the Stark-shift cancellation wavelength of strontium near 813 nm [47]. In the lattice, the atoms are spin-polarized to either the  $m_f = +9/2$  or  $-9/2$  level of the ground state. The polarization of the sample is purified by a short  $\pi$  pulse on the clock transition in a homogeneous magnetic bias field and subsequent removal of remaining ground state atoms.

After removing high-energy atoms from the lattice by temporarily reducing the lattice depth [12], the clock transition is interrogated in a bias field of about 25  $\mu\text{T}$ . The excitation probability is estimated from the atoms in ground and excited state after the interrogation. To derive an error signal free from linear Zeeman shift the laser is alternatingly tuned to points of maximum slope of the  $m_f = \pm 9/2$  transitions. A single sequence lasts about 1 s, or, if a dead time is introduced to reduce heat load and thermal gradients, one interrogation every 2 s is performed.

Different from our previous set-up [12], the 429 THz clock laser system interrogating the  $^{87}\text{Sr} \ ^1S_0 - ^3P_0$  clock transition was replaced such that stabilization to the cryogenic silicon cavity [41] is no longer required [48]. The new clock laser system uses a 48 cm long reference resonator made from ultra-low expansion glass [16]. It enables regular coherent interrogation of 640 ms duration, which leads to a resonance linewidth of about 1.4 Hz full-width at half-maximum.

**Sr lattice clock uncertainty contributions BBR shift:** The Stark shift caused by BBR was determined experimentally [49], and validated theoretically [50] as well as experimentally [8]. Recently, the dynamic correction factor  $\nu_{\text{dyn}}$ , reflecting the difference in frequency shift between BBR and a static electric field with equal rms amplitude, was refined [34]. In our experiment, the uncertainty due to BBR is limited by the uncertainty of the representative temperature  $T_{\text{rep}}$ . Temperature differences of 1.3 K at maximum measured between the warmest ( $T_{\text{max}}$ ) and coldest ( $T_{\text{min}}$ ) point of the appa-

ratus lead under the assumption of a uniform probability distribution of  $T_{\text{rep}}$  to the most probable temperature of  $(T_{\text{max}} + T_{\text{min}})/2 \approx 294$  K and an uncertainty of  $2.7 \times 10^{-17}$  of the fractional frequency correction of  $489.6 \times 10^{-17}$ . In addition, radiation from the hot oven reaches the atoms and we estimate a corresponding correction of  $8(8) \times 10^{-18}$  [12].

**Zeeman shifts:** The linear Zeeman shift, as well as the vector light shift, are removed by stabilizing the interrogation laser to the mean frequency of the  $m_F = \pm 9/2$  Zeeman components [51]. Moreover, this scheme provides continuous monitoring of the total magnetic field experienced by the atoms and thus enables a characterization and correction of the second-order Zeeman shift. We find a shift of  $-34(1.4) \times 10^{-18}$ . The uncertainty is governed by the uncertainty of the magnetic field derived from the line splitting. The uncertainty of the correction coefficient and the vector light shift can be neglected.

**Collisions:** Cold collisions and collisions with the background gas may cause frequency shifts. We measured the cold collision shift by variation of the atom density in the lattice and found a shift of  $0(3) \times 10^{-19}$ . From the lattice lifetime of 7 s, background gas collisions lead to a shift of  $15(15) \times 10^{-19}$  based on [52].

**Line pulling:** Line pulling is induced by overlapping transitions caused by atoms populating different levels or by polarization imperfections of the excitation laser such that not only  $\pi$ - but also  $\sigma$ -transitions are driven simultaneously. Investigation of the preparation sequence and the laser polarization as seen by the atoms allows us to assign a negligible correction with small uncertainty to the line pulling effect of  $0(1) \times 10^{-19}$ .

**Lattice light shifts:** By varying the lattice depth between the usual spectroscopy setting of  $72 E_r$  and  $110 E_r$ , with the recoil energy of the lattice  $E_r$ , we find a Stark shift cancellation frequency of  $368\,554\,471(3)$  MHz for a mutually parallel lattice polarization and magnetic field orientation. This leads to a fractional uncertainty of the shift of  $7 \times 10^{-18}$ . Besides the determination of the Stark shift cancellation frequency under the given experimental conditions of lattice polarization and orientation, possible shifts due to multi-photon and higher-order multi-pole excitations have to be accounted for [51]. Using the coefficients of [51] for E2/M1 transitions and two-photon induced light shifts (hyperpolarisability) [3], these higher-order effects cause shifts of  $0(5) \times 10^{-18}$  and  $-0.5(3) \times 10^{-18}$ , respectively.

**Tunnelling:** Resonant tunnelling in the lattice causes energy bands with finite widths that can be populated non-uniformly, which in turn causes a tunnelling-induced frequency shift. Bandwidths and corresponding shifts can be reduced by a tilt or acceleration of the lattice such that tunnelling is no longer resonant [53, 54]. As we prepare the atoms almost exclusively in the vibrational ground state in longitudinal direction and operate in a deep lattice, even a small lattice tilt of  $\theta = 0.12(5)^\circ$  present in our set-up is sufficient to reduce the uncertainty due to tunnelling to  $1 \times 10^{-18}$ .

*Probe light shift:* The highly advanced interrogation laser [16] enables long interrogation times of 640 ms. Therefore, the necessary intensity to drive a  $\pi$ -pulse and thus the light shift caused by the clock laser are very small. With the coefficient published in [55], we find less than  $1 \times 10^{-19}$  of fractional shift, which we use as uncertainty.

*Optical path length:* Changes of the optical path length between atoms and the clock laser cause a first-order Doppler shift and therefore errors in the frequency measurement. Although continuous drifts due to, e.g., slow temperature changes may not be overly harmful [56], clock-cycle-synchronous vibrations or rf heating of the AOM may. Lattice clocks offer the unique opportunity to stabilize the optical path length from the interrogation laser to the atom position determined by the mirror that forms the standing wave of the 1D lattice. Evaluation of the lock signal [56] reveals an upper limit of path length-induced shifts of  $1 \times 10^{-19}$ .

*Servo error:* In practice, all reference cavities used to build narrow bandwidth lasers exhibit a frequency drift due to ageing of the resonator materials and residual temperature variations. Any drift of the clock laser frequency causes a servo error, since frequency corrections are applied discontinuously. We reduce this effect by continuously sweeping the laser frequency with a rate that is updated from the atomic signal. Then, only non-linearities in the drift cause a servo error. As our new reference cavity shows an exceptionally linear drift, the fractional uncertainty is below  $10^{-18}$ .

*DC Stark shift:* Static electric fields in the interrogation region, for instance produced by patch charges on isolating surfaces, can cause substantial frequency shifts [56]. We have evaluated possible offset fields from the analysis of the observed Stark shift induced by intentionally applied electric fields. With an upper limit for the offset field of about 16(1) V/m, we expect a DC Stark shift of about  $2 \times 10^{-18}$ , which we take as uncertainty [12].

**Theory of data extrapolation** For the analysis we use the normalized frequency fluctuations  $y(t)$  defined as

$$y(t) = \frac{\nu(t) - \nu_0}{\nu_0} \quad (1)$$

with the frequency  $\nu(t)$  and the nominal frequency  $\nu_0$ . These fractional quantities allow to simply compare fluctuations between oscillators of different average frequencies with frequency ratio  $\beta = \nu_0^{(a)} / \nu_0^{(b)}$ .

$$\frac{\nu^{(a)}(t)/\nu^{(b)}(t) - 1}{\nu_0^{(a)}/\nu_0^{(b)}} \approx \frac{\nu^{(a)}(t) - \beta\nu^{(b)}(t)}{\nu_0^{(a)}} = y^{(a)}(t) - y^{(b)}(t). \quad (2)$$

To express the uncertainty introduced by the extrapolation, we follow an approach similar to the one used to relate Allan deviations and the oscillator frequency noise spectrum (see e.g. [57] and references therein). Averaging the flywheel frequency  $y(t)$  over one set of time

intervals  $\mathbb{T}_i$  with total duration  $T_i$  can be written as

$$\bar{y}_{\mathbb{T}_i} = \int_{-\infty}^{\infty} y(t)g_{\mathbb{T}_i}(t)dt, \quad (3)$$

with the weighting function  $g_{\mathbb{T}_i}(t)$ :

$$g_{\mathbb{T}_i}(t) = \begin{cases} 1/T_i & \text{for } t \in \mathbb{T}_i \\ 0 & \text{elsewhere} \end{cases}. \quad (4)$$

A similar approach is used for atomic clocks to describe the atoms' response to frequency fluctuations of the interrogation oscillator [58]. Replacing the weighting function in Eq. 3 with the combined one  $g(t) = g_{\mathbb{T}_1}(t) - g_{\mathbb{T}_2}(t)$  yields the difference  $\delta y_{\text{ext}} = \bar{y}_{\mathbb{T}_1} - \bar{y}_{\mathbb{T}_2}$  of the mean flywheel frequencies averaged over the two sets of time intervals  $\mathbb{T}_1$  and  $\mathbb{T}_2$ .

The uncertainty  $u_{\text{ext}}$  due to extrapolating the mean flywheel frequency from  $\mathbb{T}_1$  to  $\mathbb{T}_2$  is given by the standard deviation of this difference  $\delta y_{\text{ext}}$ :

$$u_{\text{ext}}^2 = \langle (\delta y_{\text{ext}})^2 \rangle. \quad (5)$$

Parseval's theorem relates this variance to the single-sided power spectral density  $S(f)$  of the flywheel oscillator's frequency fluctuations as:

$$u_{\text{ext}}^2 = \int_0^{\infty} S(f) |G(f)|^2 df, \quad (6)$$

with  $G(f) = \int_{-\infty}^{\infty} g(t) \exp(-2\pi i f t) dt$  being the Fourier transform of the weighting function. Note that the intervals  $\mathbb{T}_1$  and  $\mathbb{T}_2$  can deliberately be chosen symmetric about their common center-of-gravity. In this case, a pure linear drift of  $y(t)$  will lead to a coincidence of  $\bar{y}_{\mathbb{T}_1}$  and  $\bar{y}_{\mathbb{T}_2}$ . Thus,  $\delta y_{\text{ext}}$  and  $u_{\text{ext}}$  will not be affected by the linear drift of the flywheel oscillator.

**Model of maser spectrum** Based on the observed maser frequency fluctuations after removing a linear frequency drift of  $1.1 \times 10^{-16}$  /day, the fractional instability of the maser  $\sigma_H(\tau)$  was modelled by three noise contributions that have been added in quadrature: A contribution of  $1.18 \times 10^{-13} \cdot \tau^{-1}$  from white phase noise, a white frequency noise part of  $3.5 \times 10^{-14} \cdot \tau^{-1/2}$  and a flicker floor of  $3 \times 10^{-16} \cdot \tau^0$  [59, 60]. These values were converted to corresponding spectral power densities of frequency fluctuations [57] that were used in the calculation of  $u_{\text{ext}}$  using Eq. 6.

## ACKNOWLEDGMENTS

We gratefully acknowledge Andreas Bauch for helpful discussions. This work was supported by the Centre of Quantum Engineering and Space-Time Research (QUEST), the German Research Foundation (DFG) through the RTG 1729 'Fundamentals and Applications of ultra-cold Matter' and the CRC 1128 geo-Q 'Relativistic geodesy and gravimetry with quantum sensors',

and the project ‘International time-scales with Optical Clocks’ (ITOC), which is part of the European Metrology Research Programme (EMRP). The EMRP is jointly funded by the EMRP participating countries within EURAMET and the European Union.

---

[1] “On the future revision of the SI,” <http://www.bipm.org/en/measurement-units/new-si/> (2014).

[2] C. W. Chou, D. B. Hume, J. C. J. Koelemeij, D. J. Wineland, and T. Rosenband, *Phys. Rev. Lett.* **104**, 070802 (2010).

[3] R. Le Targat, L. Lorini, Y. Le Coq, M. Zawada, J. Guéna, M. Abgrall, M. Gurov, P. Rosenbusch, D. G. Rovera, B. Nagórny, R. Gartman, P. G. Westergaard, M. E. Tobar, M. Lours, G. Santarelli, A. Clairon, S. Bize, P. Laurent, P. Lemonde, and J. Lodewyck, *Nature Com.* **4**, 2109 (2013).

[4] P. Dubé, A. A. Madej, Z. Zhou, and J. E. Bernard, *Phys. Rev. A* **87**, 023806 (2013).

[5] N. Hinkley, J. A. Sherman, N. B. Phillips, M. Schioppo, N. D. Lemke, K. Beloy, M. Pizzocaro, C. W. Oates, and A. D. Ludlow, *Science* **341**, 1215 (2013).

[6] B. J. Bloom, T. L. Nicholson, J. R. Williams, S. L. Campbell, M. Bishof, X. Zhang, W. Zhang, S. L. Bromley, and J. Ye, *Nature* **506**, 71 (2014).

[7] N. Huntemann, B. Lipphardt, C. Tamm, V. Gerginov, S. Weyers, and E. Peik, *Phys. Rev. Lett.* **113**, 210802 (2014).

[8] I. Ushijima, M. Takamoto, M. Das, T. Ohkubo, and H. Katori, *Nature Photonics* **9**, 185 (2015).

[9] F. Riehle, *C. R. Physique* **16**, 506 (2015), special issue: The measurement of time / La mesure du temps.

[10] H. Margolis, *Nature Physics* **10**, 82 (2014), commentary.

[11] P. Gill and F. Riehle, in *Proceedings of the 2006 Meeting of the European Frequency and Time Forum* (available under: <http://www.eftf.org/proceeding/index.html>, Braunschweig, 2006) pp. 282–288.

[12] S. Falke, N. Lemke, C. Grebing, B. Lipphardt, S. Weyers, V. Gerginov, N. Huntemann, C. Hagemann, A. Al-Masoudi, S. Häfner, S. Vogt, U. Sterr, and C. Lisdat, *New J. Phys.* **16**, 073023 (2014).

[13] T. E. Parker, *Rev. Sci. Instrum.* **83**, 021102 (2012).

[14] A. Bauch, S. Weyers, D. Piester, E. Staliuniene, and W. Yang, *Metrologia* **49**, 180 (2012).

[15] L. Śliwczynski, P. Krehlik, A. Czubla, L. Buczak, and M. Lipiński, *Metrologia* **50**, 133 (2013).

[16] S. Häfner, S. Falke, C. Grebing, S. Vogt, T. Legero, M. Merimaa, C. Lisdat, and U. Sterr, *Opt. Lett.* **40**, 2112 (2015).

[17] A. Al-Masoudi, S. Dörscher, S. Häfner, U. Sterr, and C. Lisdat, “Noise and instability of an optical lattice clock,” arXiv:1507.04949v2 [physics.atom-ph] (2015), subm. to PRA.

[18] V. Gerginov, N. Nemitz, S. Weyers, R. Schröder, R. D. Griebsch, and R. Wynands, *Metrologia* **47**, 65 (2010).

[19] S. Weyers, V. Gerginov, N. Nemitz, R. Li, and K. Gibble, *Metrologia* **49**, 82 (2012).

[20] W.-K. Lee, D.-H. Yu, C. Y. Park, and J. Mun, *Metrologia* **47**, 24 (2010).

[21] CIPM, “Report of the 101<sup>th</sup> meeting of the Comité International des Poids et Mesures (CIPM),” Bureau International des Poids et Mesures (BIPM), Sevres, Paris Cedex (2013).

[22] M. M. Boyd, A. D. Ludlow, S. Blatt, S. M. Foreman, T. Ido, T. Zelevinsky, and J. Ye, *Phys. Rev. Lett.* **98**, 083002 (2007).

[23] X. Baillard, M. Fouché, R. L. Targat, P. G. Westergaard, A. Lecallier, F. Chapelet, M. Abgrall, G. D. Rovera, P. Laurent, P. Rosenbusch, S. Bize, G. Santarelli, A. Clairon, P. Lemonde, G. Grosche, B. Lipphardt, and H. Schnatz, *Eur. Phys. J. D* **48**, 11 (2008).

[24] G. K. Campbell, A. D. Ludlow, S. Blatt, J. W. Thomsen, M. J. Martin, M. H. G. de Miranda, T. Zelevinsky, M. M. Boyd, J. Ye, S. A. Diddams, T. P. Heavner, T. E. Parker, and S. R. Jefferts, *Metrologia* **45**, 539 (2008).

[25] F.-L. Hong, M. Masha, M. Takamoto, H. Inaba, S. Yanagimachi, A. Takamizawa, K. Watabe, T. Ikegami, M. Imae, Y. Fujii, M. Amemiya, K. Nakagawa, K. Ueda, and H. Katori, *Opt. Lett.* **34**, 692 (2009).

[26] S. Falke, H. Schnatz, J. S. R. Vellore Winfred, T. Middelmann, S. Vogt, S. Weyers, B. Lipphardt, G. Grosche, F. Riehle, U. Sterr, and C. Lisdat, *Metrologia* **48**, 399 (2011).

[27] A. Yamaguchi, N. Shiga, S. Nagano, Y. Li, H. Ishijima, H. Hachisu, M. Kumagai, and T. Ido, *Appl. Phys. Express* **5**, 022701 (2012).

[28] K. Matsubara, H. Hachisu, Y. Li, S. Nagano, C. Locke, A. Nohgami, M. Kajita, K. Hayasaka, T. Ido, and M. Hosokawa, *Opt. Express* **20**, 22034 (2012).

[29] D. Akamatsu, H. Inaba, K. Hosaka, M. Yasuda, A. Onae, T. Suzuyama, M. Amemiya, and F.-L. Hong, *Appl. Phys. Express* **7**, 012401 (2014).

[30] H. Hachisu, M. Fujieda, S. Nagano, T. Gotoh, A. Nogami, T. Ido, S. Falke, N. Huntemann, C. Grebing, B. Lipphardt, C. Lisdat, and D. Piester, *Opt. Lett.* **39**, 4072 (2014).

[31] Y.-G. Lin, Q. Wang, Y. Li, F. Meng, B.-K. Lin, E.-J. Zang, Z. Sun, F. Fang, T.-C. Li, and Z.-J. Fang, *Chin. Phys. Lett.* **32** (2015), 10.1088/0256-307X/32/9/090601.

[32] H. Hachisu and T. Ido, “Intermittent optical frequency measurements to reduce the dead time uncertainty of frequency link,” arXiv:1508.05996 (2015).

[33] T. Tanabe, D. Akamatsu, T. Kobayashi, A. Takamizawa, S. Yanagimachi, T. Ikegami, T. Suzuyama, H. Inaba, S. Okubo, M. Yasuda, F.-L. Hong, A. Onae, and K. Hosaka, “Improved frequency measurement of the  $^1S_0$ - $^3P_0$  clock transition in  $^{87}\text{Sr}$  using the Cs fountain clock at NMIJ as a transfer oscillator,” arXiv:1509.03967 [physics.atom-ph] (2015).

[34] T. L. Nicholson, S. L. Campbell, R. B. Hutson, G. E. Marti, B. J. Bloom, R. L. McNally, W. Zhang, M. D. Barrett, M. S. Safronova, G. F. Strouse, W. L. Tew, and J. Ye, *Nature Com.* **6**, 6896 (2015).

[35] J. Leute, N. Huntemann, B. Lipphardt, C. Tamm, P. B. R. Nisbet-Jones, S. A. King, R. M. Godun, J. M. Jones, H. S. Margolis, P. B. Whibberley, A. Wallin,

M. Merimaa, P. Gill, and E. Peik, "Frequency comparison of  $^{171}\text{Yb}^+$  ion optical clocks at PTB and NPL via GPS PPP," arXiv:1507.04754v1 [physics.atom-ph] (2015).

[36] D.-H. Yu, M. Weiss, and T. E. Parker, *Metrologia* **44**, 91 (2007).

[37] R. J. Douglas and J.-S. Boulanger, in *Proc. 11th European Frequency and Time Forum (EFTF), 4-7 March 1997, Neuchâtel, Switzerland* (1997) pp. 345–349.

[38] "BIPM CircularT," Monthly, available at: <http://www.bipm.org/jsp/en/TimeFtp.jsp>.

[39] J. G. Hartnett, N. R. Nand, and C. Lu, *Appl. Phys. Lett.* **100**, 183501 (2012).

[40] R. Storz, C. Braxmaier, K. Jäck, O. Pradl, and S. Schiller, *Opt. Lett.* **23**, 1031 (1998).

[41] T. Kessler, C. Hagemann, C. Grebing, T. Legero, U. Sterr, F. Riehle, M. J. Martin, L. Chen, and J. Ye, *Nature Photonics* **6**, 687 (2012).

[42] C. Hagemann, C. Grebing, C. Lisdat, S. Falke, T. Legero, U. Sterr, F. Riehle, M. J. Martin, and J. Ye, *Opt. Lett.* **39**, 5102 (2014).

[43] M. J. Thorpe, L. Rippe, T. M. Fortier, M. S. Kirchner, and T. Rosenband, *Nature Photonics* **5**, 688 (2011).

[44] G. Panfilo and T. E. Parker, *Metrologia* **47**, 552 (2010).

[45] L. Cacciapuoti and C. Salomon, *Eur. Phys. J. Special Topics* **172**, 57 (2009).

[46] G. P. Barwood, P. Gill, G. Huang, and H. A. Klein, *Meas. Sci. Technol.* **23**, 055201 (2012).

[47] H. Katori, M. Takamoto, V. G. Pal'chikov, and V. D. Ovsiannikov, *Phys. Rev. Lett.* **91**, 173005 (2003).

[48] C. Hagemann, C. Grebing, T. Kessler, S. Falke, N. Lemke, C. Lisdat, H. Schnatz, F. Riehle, and U. Sterr, *IEEE Trans. Instrum. Meas.* **62**, 1556 (2013).

[49] T. Middelmann, C. Lisdat, S. Falke, J. S. R. Vellore Winfred, F. Riehle, and U. Sterr, *IEEE Trans. Instrum. Meas.* **60**, 2550 (2011).

[50] M. S. Safronova, S. G. Porsev, U. I. Safronova, M. G. Kozlov, and C. W. Clark, *Phys. Rev. A* **87**, 012509 (2013).

[51] P. G. Westergaard, J. Lodewyck, L. Lorini, A. Lecallier, E. A. Burt, M. Zawada, J. Millo, and P. Lemonde, *Phys. Rev. Lett.* **106**, 210801 (2011).

[52] K. Gibble, *Phys. Rev. Lett.* **110**, 180802 (2013).

[53] P. Lemonde and P. Wolf, *Phys. Rev. A* **72**, 033409 (2005).

[54] C. Sias, H. Lignier, Y. P. Singh, A. Zenesini, D. Ciampini, O. Morsch, and E. Arimondo, *Phys. Rev. Lett.* **100**, 040404 (2008).

[55] X. Baillard, M. Fouché, R. Le Targat, P. G. Westergaard, A. Lecallier, Y. Le Coq, G. D. Rovera, S. Bize, and P. Lemonde, *Opt. Lett.* **32**, 1812 (2007).

[56] S. Falke, M. Misera, U. Sterr, and C. Lisdat, *Appl. Phys. B* **107**, 301 (2012).

[57] S. T. Dawkins, J. J. McFerran, and A. N. Luiten, *IEEE Trans. Ultrason. Ferroelectr. Freq. Control* **54**, 918 (2007).

[58] G. J. Dick, in *Proceedings of 19<sup>th</sup> Annu. Precise Time and Time Interval Meeting, Redondo Beach, 1987* (U.S. Naval Observatory, Washington, DC, 1988) pp. 133–147.

[59] T. E. Parker, in *Proceedings of the 1999 Joint Meeting of the European Frequency and Time Forum and The IEEE International Frequency Control Symposium* (1999) pp. 173–176.

[60] V. Vorontsov, A. Belyaev, and N. Demidov, in *Materials of the VI symposium "metrology of time and space" 2012* (2012).